THE ASTRONOMICAL JOURNAL, 122:1538–1544, 2001 September
© 2001. The American Astronomical Society. All rights reserved. Printed in U.S.A.

HUBBLE SPACE TELESCOPE AND GROUND-BASED SPECTROSCOPY OF K648 IN M15[1]

LUCIANA BIANCHI,[2,3] RALPH BOHLIN,[4] GIOVANNI CATANZARO,[2] HOLLAND FORD,[2,4] AND ARTURO MANCHADO[5,6]

Received 2001 April 24; accepted 2001 May 31

ABSTRACT

We derive some element abundances for the central star of the planetary nebula K648 from analysis of *Hubble Space Telescope* Faint Object Spectrograph spectra (1200–3300 Å). Carbon is found to be approximately 4 times overabundant with respect to solar values, while oxygen is underabundant and silicon about solar, and He/H = 0.6. The stellar continuum indicates a reddening of $E(B-V) = 0.08$ and is well approximated by a synthetic model with $T_{\rm eff} = 37{,}000$ K and $\log g = 4.0$, as found previously by Heber, Dreizler, & Werner. The scaling of the synthetic model with the measured UV flux indicates $R = 1.3\ R_\odot$, and thus $\log(L/L_\odot) = 3.45$, $M = 0.62\ M_\odot$, assuming a distance of $D = 10.3$ kpc. The C IV exhibits a wind profile, from which a terminal wind velocity of $V_\infty = 1600 \pm 150$ km s^{-1} is derived and a column density of N_i(C IV) $= 6 \pm 3 \times 10^{15}$ cm^{-2}. From ground-based spectra obtained at the William Hershel 4.2 m telescope we derive the first measurement of the expansion velocity for the nebula: $V_{\rm exp}$([N II]) $= 11.9$ km s^{-1} and $V_{\rm exp}(\mathrm{H}\alpha) = 16.7$ km s^{-1}. Combined with the nebular radius measured from *HST* imaging in our previous paper, the velocity yields an expansion age of the object $\mathrm{Age}_{\rm kinematic} \geq 4270$ yr. This value is slightly higher than predictions from post-AGB evolutionary models for a $\approx 0.6\ M_\odot$ He-burning remnant. The photospheric overabundance of He and C, as well as the low luminosity of the central star, are consistent with a post-AGB object that experienced a late thermal pulse and consequent third dredge-up, and which is now in a luminosity-dip He-burning phase. The progenitor mass is fairly low.

Key words: planetary nebulae: individual (K648) — stars: abundances — stars: AGB and post-AGB

1. INTRODUCTION

Only 12 of the known Galactic planetary nebulae (PNs) are associated with the Galactic halo, and four of them are in globular clusters (Howard, Henry, & McCartney 1977; Gillet et al. 1989; Jacoby et al. 1997). These rare objects offer important clues to many aspects of stellar evolution: (1) post-AGB evolution at very low metallicity, (2) generally low progenitor masses, and (3) the importance of the binary mechanism (PNs originating from common envelope evolution) in the globular cluster (GC) environment, where mechanisms and conditions for formation and survival of binary systems differ significantly from the general field.

The object of this study, K648, was the first PN discovered in a GC (M15) and thus has been the subject of numerous investigations. While the association with the GC M15 provides an independent and reliable measurement of its distance, and thus absolute energy parameters can be derived much more accurately than is usually possible for isolated Galactic PN, the location in the GC crowded field and fairly large distance make ground-based measurements uncertain. The *Hubble Space Telescope's* (*HST*) spatial resolution provided the first detailed morphology for this object (Bianchi et al. 1995, hereafter Paper I; Alves, Bond, & Livio 2000, hereafter ABL00), displaying an inner bipolar structure with an extended more spherical fainter halo, and a first reliable measure of its size. A compilation of relevant parameters that will be used in our analysis, extracted from the abundant literature on this object, as well as values derived in this work, is given in Table 1.

In this paper we present UV spectroscopy of the central star of K648, obtained with the *HST* Faint Object Spectrograph (FOS) and use it to study the stellar photospheric and wind lines and the UV continuum distribution and to determine photospheric abundances (§ 3.1) and wind velocity (§ 3.2). Additionally, high-resolution profiles of optical nebular emission lines were obtained at the 4.2 m William Hershel Telescope (WHT) to study the gas kinematics (§ 4). The expansion velocity is used to estimate a dynamical age for the nebular shell, for comparison with the evolutionary age of the central star.

2. THE OBSERVATIONS

2.1. *HST Spectroscopy*

UV spectroscopy in the range 1150–3300 Å was obtained with the *HST* FOS, as part of a GTO program (PI: H. Ford). The range was covered with three separate exposures of the gratings G130H, G190H, and G270H (data sets Y1C40105T, Y1C40104T, and Y1C40103P), with resolution of approximately 1, 1.5, and 2 Å, respectively. The 0.″83 aperture was used.

The FOS observations are flux calibrated on the white dwarf scale according to Bohlin (1996) and Bohlin, Lindler, & Keyes (1995). Analysis of a confirmation picture obtained in the FOS 3.″7 × 3.″7 acquisition aperture demonstrates that the blind offset pointing maneuver from the offset star to K648 was accurate to less than 0.″1. The offset star was acquired in the FOS binary acquisition mode. The uncer-

[1] Based on observations with the NASA/ESA *Hubble Space Telescope*, obtained at the Space Telescope Science Institute, which is operated by the Association of Universities for Research in Astronomy (AURA), Inc., under NASA contract NAS 5-26555, and on observations made with the William Hershel Telescope (WHT), operated on the island of La Palma by the Royal Greenwich Observatory in the Spanish Observatorio del Roque de Los Muchachos of the Instituto de Astrofísica de Canarias.

[2] Center for Astrophysical Sciences, Johns Hopkins University, 239 Bloomberg Center for Physics & Astronomy, 3400 North Charles Street, Baltimore, MD 21218.

[3] Osservatorio Astronomico di Torino, I-10025 Pino Torinese, Italy.

[4] Space Telescope Science Institute, 3700 San Martin Drive, Baltimore, MD 21218.

[5] Instituto de Astrofisica de Canarias, via Láctea, E-38200 La Laguna, Tenerife, Spain.

[6] Consejo Superior de Investigaciones Cientificas, Spain.

TABLE 1

NEBULAR AND STELLAR PARAMETERS OF K648

Quantity	Value	References
Names	K648, PK 065-27 1; PN Aro 111; Ps 1	
Distance to M15 (kpc)	9.7; 10.3; 12.3	Webbink 1985; ABL00; Harris 1996
Rad. Velocity (km s^{-1})	-140.6 ± 16.9	Schneider et al. 1983
log Hβ flux	-12.08; -12.13; -12.18	Peimbert 1973; Hawley & Miller 1978; Torres-Peimbert & Peimbert 1979
$E(B-V)$	0.1; 0.08; $0.13 \pm .05$; 0.08	Torres-Peimbert & Peimbert 1979; Adams et al. 1984; ABL00, this work
Nebular N_e (cm^{-3})	3020; 1700	Kingsburgh & Barlow 1992; Adams et al. 1984
Nebular T_e (K)	12,000; 10,800; 10,600	Torres-Peimbert & Peimbert 1979; Adams et al. 1984
Diameter (arcsec)	≤ 1, 3.5, 5	Adams et al. 1984; Aurière & Cordoni 1981; Bianchi et al. 1995
$M_{\rm ionized\ gas}$ ($M_\odot$)	0.011, 0.07	Adams et al. 1984; Bianchi et al. 1995
$V_{\rm expansion}$([N II]) (km s^{-1})	11.9	This work
$V_{\rm expansion}$(Hα) (km s^{-1})	16.7	This work
$\rm Age_{kinematic}$ (yr)	≥ 4270	This work
V (mag)	14.95	Aurière & Cordoni 1981
$T_{\rm eff}$ (K)	37,000;[a] 35,000;[b] 35,000;[b] 28,000;[c] 32,000;[d] 40,000;[e] 35,000[b]	Heber et al. 1993; Adams et al. 1984; Bianchi et al. 1995; Adams et al. 1984; Peña, Torres-Peimbert, & Perinotto 1992;
log g	4.0	Heber et al. 1993
R_* ($R_\odot$)	1.3	This work
M_* ($M_\odot$)	0.60, 0.58, 0.62	ABL00; Bianchi et al. 1995; this work
log($L/L_\odot$) (blackbody)	3.78, 3.67, 3.45	ABL00; Bianchi et al. 1995; this work
$V_{\rm esc}$ (km s^{-1})	425	This work
He/H	0.5; 0.6	Heber et al. 1993; this work
Oxygen abundance (resp. solar)	Underabundant	Heber et al. 1993; this work
Carbon abundance (resp. solar)	3/1, 4/1	Heber et al. 1993; this work
Silicon abundance (resp. solar)	1.6/1	This work
V_∞ (km s^{-1})	2100, 1600, 1600 ± 150	Adams et al. 1984; Bianchi et al. 1995; this work
N_i(C IV)-wind (cm^{-2})	$6 \pm 3 \times 10^{15}$	This work
$\dot{M}$ ($M_\odot$ yr^{-1}) $\times$ Q_i(C IV)	$3.2 \pm 1.1 \times 10^{-11}$	This work

[a] Stellar temperature determination based on NLTE model atmosphere method.
[b] UV color temperature method.
[c] Zanstra[H] method.
[d] Zanstra[He] method.
[e] Stoy method.

tainty in FOS absolute fluxes should be better than $\approx 5\%$ for point sources, when the target acquisition and signal-to-noise ratio (S/N) are as good as our K648 observations.

In Figure 1 we compare the FOS spectrum with *IUE* archive observations used previously by several authors (e.g., Paper I and references therein). We show data sets SWP9605, SWP17069, and LWP13360 combined from the *IUE* archive, which were analyzed in Paper I. The *IUE* fluxes are corrected to the FOS scale according to the FLXCOR procedure of Bohlin (1996) for accurate comparison.

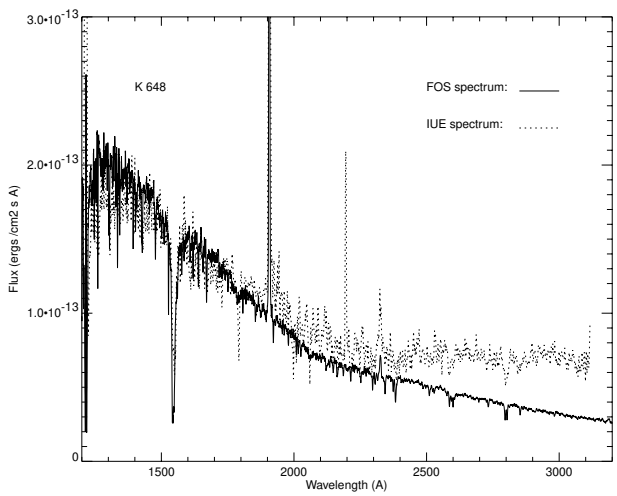

FIG. 1.—Comparison of FOS (*solid line*) and *IUE* (*dotted line*) ultraviolet spectra. The mismatch in flux is discussed in the text. The excess at long wavelengths in the *IUE* fluxes is due to contamination by cooler nearby stars included in the large aperture.

Figure 1 shows that the *IUE* fluxes are higher than the FOS fluxes at long wavelengths (≥ 1800 Å), while at shorter wavelengths the *IUE* fluxes are up to $\approx 15\%$ lower than the FOS fluxes. At long wavelengths, the difference is most likely caused by contamination from cooler field stars in the $10'' \times 20''$ *IUE* slit, which has 200 times the area of the $\approx 1''$ circular FOS aperture and includes several fields stars, as can be seen from the *HST* imaging (Paper I). We found no clear explanation for the difference at shorter wavelengths, which is within 2–3 σ of the expected agreement between the two measurements. Perhaps the *IUE* target acquisition in such a crowded field as M15 was off by 2″–3″, which could cause a few percent loss of flux in the slit. The FOS spectrum is used in §§ 3.1 and 3.2 to derive photospheric abundances and wind parameters.

2.2. *Ground-based Spectroscopy*

High-resolution long-slit spectra were obtained with the Utrecht Echelle Spectrograph (UES) on the WHT during service time on 1994 August 19. We used the 79 line mm^{-1} echelle grating and a 700 mm focal length camera. The reciprocal dispersion was 2.92 Å mm^{-1} at 6560 Å. The slit was located at a position angle of 324° and was 0.″8 wide and 6″ long. A 1024×1024 Tektronix CCD was used with a pixel size (24 μm) equivalent to ~ 3.21 km s^{-1} along the

dispersion and 0.″36 along the spatial direction. The instrumental FWHM was 5.4 $\pm$ 0.3 km s^{-1}. The seeing was better than 1″.

The data were reduced with standard IRAF routines. Wavelength calibration accuracy is better that 0.2 km s^{-1}. The one-dimensional spectrum, shown in Figure 5, was obtained by adding up 5.″3 (the extension of the nebula). These data are used in § 4 to measure the expansion velocity.

3. THE STELLAR PARAMETERS

The UV FOS spectrum of the central star (Fig. 2) contains a wealth of photospheric lines. All the He II transitions that fall in this range are clearly detected in the spectrum (He II $\lambda\lambda$1640, 2136, 2149, 2165, 2187, 2215, 2253, 2306, 2385, 2511, 2734), as well as strong C III lines ($\lambda\lambda$1385, 1427, 1577, 1620, 1645, 1923, 2297, 2698). Some of these lines are blended with other transitions. Weaker C IV lines are also present (see Fig. 3) at $\lambda\lambda$2525, 2530 (the latter probably blended with a C II transition). Below we use the most reliable lines (shown in Fig. 3) to derive some element abundances. The resonance doublet of C IV displays a strong P Cygni profile (Fig. 4) and is the only wind feature detected in the spectrum. It will be discussed in § 3.2. The strong C II 1335 lines (resonance) are mostly of interstellar origin, given the temperature of this star, and thus will not be used in the analysis that follows.

3.1. *Stellar Abundances*

In this section we determine atmospheric chemical abundances of some elements by LTE spectral modeling of the strongest photospheric lines in the ultraviolet spectrum. Previous quantitative spectroscopic analysis by Heber, Dreizler, & Werner (1993), including both optical (Calar Alto) and UV (*HST*-GHRS) spectra, yielded the stellar parameters $T_{\rm eff}$ = 37,000 K, $\log g$ = 4.0, $n_{\rm He}/n_{\rm H}$ = 0.5 and a carbon abundance of 3 times the solar value. Our FOS spectra cover a wider UV range than the GHRS spectra analyzed by Heber at al., however at lower resolution. We use $T_{\rm eff}$ and $\log g$ from these authors, because $\log g$ was determined from the wings of their Hγ and Hδ lines and $T_{\rm eff}$ from the C III to C IV ratio.

We computed model (synthetic) spectra, using (1) ATLAS9 (Kurucz 1993) to compute atmosphere models

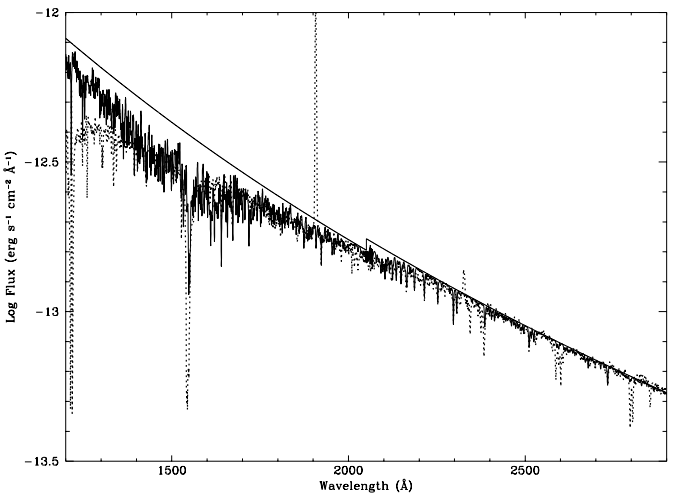

FIG. 2.—Comparison between observed flux (*dotted line*) and synthetic model (*solid line*) computed for $T_{\rm eff}$ = 37,000 K and $\log g$ = 4.0. The smooth solid line is the underlying photosphere.

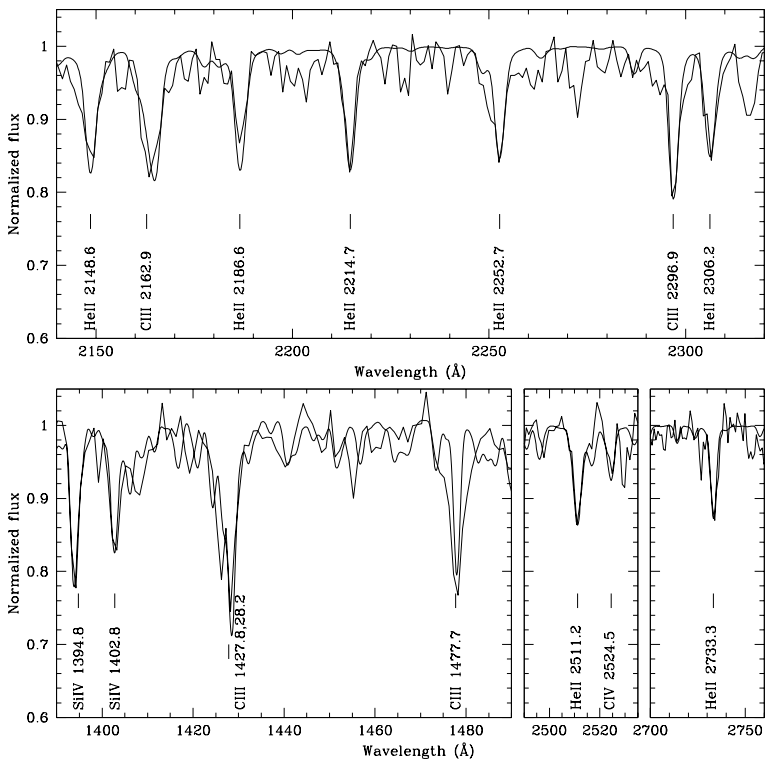

FIG. 3.—Portions of the FOS spectrum (*thick line*) and synthetic spectrum (*thin line*) showing the most relevant lines. Abundances of He, Si, and C have been derived by fitting the strength of the observed lines (*marked*). The abundance values are given in Table 2.

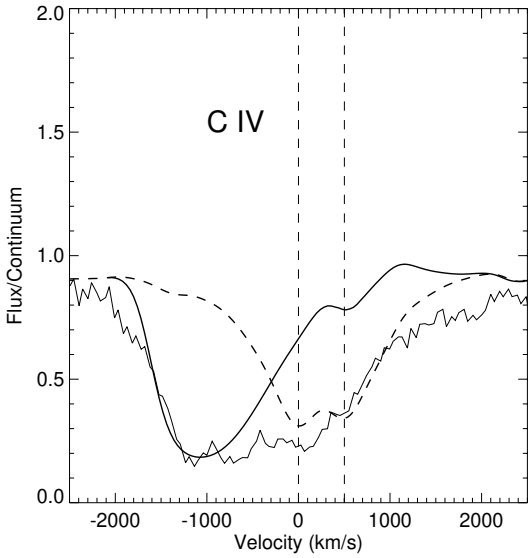

FIG. 4.—C IV resonance doublet and the best-fit wind profile calculated with the SEI code (*thick line*). The thick dashed line is the photospheric profile from the model described in the text. The vertical dashed lines mark the rest position of the two components of the doublet. The terminal velocity is $V_\infty = 1600 \pm 150$ km s^{-1}.

and (2) SYNTHE (Kurucz & Avrett 1981) to calculate the emerging spectrum, for comparison with the observed lines, varying the element abundances to fit the observed spectrum.

For the transitions, we have adopted the atomic parameters from the Kurucz (1993) line list.

In Figure 2 we show the observed and best-fit model fluxes over the entire FOS range to compare the continuum flux distributions. Both the underlying photospheric flux (*solid line*) and the emergent flux from the synthetic model are shown. In this figure, the observed FOS flux has been dereddened with $E(B-V) = 0.08$ and corrected for the nebular contribution to the continuum emission to compare the intrinsic, pure stellar flux to the model. The value of $E(B-V) = 0.08$ has been chosen to best remove the 2200 Å extinction feature. It is the average of most determinations found in the literature (see references in Aurière, Adams, & Seaton 1983) and of more recent values quoted in Table 1, although ABL00 found $E(B-V) = 0.13$ and Hawley & Miller (1978) adopted $E(B-V) = 0.20$ from the Balmer decrement. These higher values produce a significant excess around 2200 Å and were therefore excluded. The nebular continuum has been computed including H and He recombination and two-photon emission processes, assuming $N_e = 2{,}500$ cm^{-3} and $T_e = 11{,}000$ K, and scaled to absolute values using the measured Hβ flux as follows. Correcting for $c = 0.12$ [$E(B-V) = 0.08$], the total Hβ flux measured at the earth is $\log F\beta = -12.0$. This emission comes from an area of about 3.″5 diameter (Paper I), so the value was further scaled to the area entering the FOS 1″ aperture. The computed nebular continuum emission amounts to a few percent of the total flux at the longest wavelengths, where it is largest, so it is a very small correction. In Figure 2, we can see that the computed synthetic spectrum reproduces the observed flux very well, except for the shortest wavelength range (<1400 Å). Numerous iron lines contribute significantly to the conspicuous blanketing of the photospheric flux below ~1800 Å. No strong resolved Fe lines are available for precise abundance determination; however, the good match to the observed continuum slope shown in Figure 2 shows that the solar Fe abundance assumed in the model is appropriate. For lower Fe abundances the synthetic spectrum has higher flux than the observed spectrum shortward of 1800 Å. Therefore, we can qualitatively conclude that there is no evidence for Fe underabundance. This seems very surprising given the low metallicity of M15 ([Fe/H] = −2.25; Harris 1996). However, Behr, Cohen, & McCarthy (2000), in an analysis of 18 blue horizontal-branch (BHB) stars in M15 found photospheric compositions to vary strongly with temperature. Most of their BHB stars with $T_{\rm eff} \geq 10{,}000$ K have solar abundance of iron ([Fe/H] ≈ 0), i.e., an enhancement by over a factor of 300 with respect to cooler stars in the cluster. Behr et al. (2000) suggest an element diffusion mechanism as a possible—at least partial—explanation, regulated by rotation (because the two hot BHB stars not showing Fe enhancement rotate twice as fast as the others in their sample).

The strong observed absorption lines not reproduced by the model in Figure 2 are of interstellar origin. A mismatch between the observed and synthetic spectrum remains in the G130H range. Lowering the gravity value would decrease the emergent synthetic spectrum flux at short wavelengths; however, it also produces a significant mismatch with the observed fluxes throughout the FOS range. Therefore, we have no explanation for the mismatch at short wavelengths, and we find that the Heber et al. values of $T_{\rm eff}$ and $\log g$ give the best-fit model.

We also fitted the line spectrum with an iterative procedure, to determine abundances of the observed species. In Figure 3 the portions of the spectrum with the strongest photospheric lines are shown, as well as the best-fit synthetic spectrum. The element abundances derived by fitting the observed lines are given in Table 2, in the form of N/H by number. Uncertainties in abundances come from uncertainties of $T_{\rm eff}$ and $\log g$, and in the continuum location. How these uncertainties affect the abundance determinations cannot be estimated in a straightforward way. Our procedure was to calculate the abundance independently from each individual line of the same element and to adopt the standard deviation around the average result as error. In this way we found a 0.1 dex error for both helium and carbon, and we adopted the same value for the abundance of silicon as well, of which only two lines are available in our range. The fact that we used an LTE model analysis should not be relevant, because all of the lines considered have an optical depth below $\log \tau \approx -4$, the limit at which the temperature distribution along the atmosphere calcu-

TABLE 2

PHOTOSPHERIC ABUNDANCES FOR K648

Element	log(N/H) K648	log(N/H) Sun
He.....	−0.2	−1.01
C	−2.7	−3.44
Si.....	−4.5	−4.45

NOTE.—Abundances are given in form of log [$N(E)/N$(H)]. Errors have been estimated to be 0.1 dex. Solar values are from Kurucz (1993).

lated under LTE assumptions shows differences from the one computed in non-LTE (NLTE). Oxygen lines that are predicted in this range by the model for solar abundance are not seen in the K648 spectrum. We therefore infer oxygen to be significantly underabundant, by at least a factor of 10 (not quantifiable because lines are not measurable).

The synthetic model fit shown in Figure 2 also yields a measure of the stellar radius over the distance R/D by scaling the computed fluxes to the dereddened spectrum. Adopting $D = 10{,}300$ pc (average from recent determinations; see Table 1) we derive $R = 1.3\ R_\odot$.

By using the value adopted in this paper of $\log g = 4.0$ and this radius, we derive $M = 0.62 \pm 0.10\ M_\odot$.

3.2. *The Wind from the Central Star*

The C IV resonance doublet at $\lambda\lambda$1548, 1552 exhibits a wind profile: a broad asymmetric blueshifted absorption with no emission. The line is shown in Figure 4 in velocity space in the rest frame of the star. The recession velocity of the star $V = -140.6 \pm 16.9$ km s^{-1} (Joy 1949; Schneider et al. 1983) has been removed from the observed spectrum. A narrow absorption component (NAC) of the doublet is also present (see Fig. 4), displaced at a velocity of $V(\mathrm{NAC}) \approx -1200$ km s^{-1}. The profile was modeled using the SEI ("Sobolev" approximation in the source function calculation and "exact integration" of the transfer equation) method originally developed by Lamers, Cerruti-Sola, & Perinotto (1987) with the parametrization of Bianchi et al. (2000). Figure 4 shows also the best-fit profile. We included in the wind profile calculations an underlying photospheric profile from the synthetic spectrum described in the previous section (also shown, *dashed line*).

The observed C IV profile has a rather complicated appearance, and the central part cannot be reproduced by the SEI code; however, the blueshifted wing yields an accurate measurement of the wind terminal velocity. From the profile fit we derive a wind velocity of $V_\infty = 1600 \pm 150$ km s^{-1} and a total optical depth for the blue component of the doublet of $\tau(\mathrm{blue}) = 3.0 \pm 1.0$. The optical depth of the red component is half that of the blue component, consistent with the ratio of their respective f-values. The large errors on the measured optical depth are mainly due to uncertainties in the continuum and to the nonsmooth shape of the profile, including the narrow absorption components. The absorption part of observed profile can be approximated with theoretical profiles with different combinations of parameters, in particular the values of the optical depth law exponents $\alpha 1$ and $\alpha 2$ (see eq. [2] of Bianchi et al. 2000).

A unique parameter combination cannot be found in this case, and the whole range of acceptable parameters has been taken into account to estimate the uncertainty of the optical depth. The C IV profile is quite different from typical P Cygni profiles of hot stars, although there is a somewhat similar case, HD 47839, studied in the UV by Groenewegen & Lamers 1989 (hereafter GL89, Fig. 2*c*). Its C IV profile has similar narrow absorption components and pronounced photospheric absorption, although not so deep as in the K648 case. HD 47839 also has a similar T_{eff} and gravity to the central star of K648. Its strange C IV profile was fitted by GL89 with somewhat extreme values of parameters. We also computed profiles with values for the parameters γ, $\alpha 1$, and $\alpha 2$ used by GL89 for HD 47839, adjusting the total optical depth and terminal velocity to fit the K648 observed line. We obtained a model profile very similar to the fit shown in Figure 4, with a slightly better match of the absorption component, but a larger mismatch to the central part. The interesting result is that, also for this combination of parameters, an optical depth $\tau(\mathrm{blue}) = 2.0$ was required to fit the profile and the same value of V_∞ as found for the other parameter combinations.

The measured optical depth translates into a wind column density for the C IV ion of $N_i(\mathrm{C\ IV}) = 6 \pm 3 \times 10^{15}$ cm^{-2}. The velocity law has an exponent $\gamma = 0.3$. The low value is required to explain the lack of emission. The Doppler width of the turbulence was found to be about 15% $\pm$ 5% of the wind terminal velocity, or $V_{\mathrm{turb}} \approx 240$ km s^{-1}. With the parameters determined from the profile fit, and a stellar radius $R = 1.3\ R_\odot$ (previous section), using eq. (21) of Groenewegen & Lamers (1989), the mass-loss rate can be determined if the ionization of carbon, $Q_i(\mathrm{C\ IV}) = N_i(\mathrm{C\ IV})/N_i(\mathrm{C})$ is known. We find $\dot{M} \times Q_i(\mathrm{C\ IV}) = 3.2 \pm 1.1 \times 10^{-11}\ M_\odot$ yr^{-1} (the error includes the uncertainties of V_∞, optical depth, and other parameters of the profile fit), for a carbon abundance 4 times higher than solar (this paper). The total mass flux is obtained by scaling the column density of C IV to the total column density of carbon and dividing by the abundance of carbon $A_E(\mathrm{C}) = N_i(\mathrm{C})/N_i(\mathrm{tot})$. Therefore, the mass-loss rate scales linearly (inversely) with the abundance of the element, so for a solar carbon abundance $\dot{M}$ would be higher by a factor of 4 (see eq. [21] of GL89).

Because the C IV line in the spectrum is not saturated, it is very likely that $Q_i(\mathrm{C\ IV})$ is much lower than 1. The wind ionization depends on the wind density and the He ionization.

The mass-loss rate expected from the radiation pressure driven theory can be estimated using the "recipe" by Kudritzki et al. (1989) or Groenewegen, Lamers, & Pauldrach (1989). For this set of stellar parameters $\dot{M} \approx 8 \times 10^{-9}\ M_\odot$ yr^{-1} is predicted, the value rapidly increasing for higher luminosities. If the theory could be extended to such a low-luminosity object, the ionization fraction of C IV then would range between 10^{-2} and 10^{-3}. Planned *Far Ultraviolet Spectroscopic Explorer* (*FUSE*) spectra will clarify the mass loss.

4. GAS DYNAMICS AND KINEMATICAL AGE

The expansion velocity was calculated from the H_α and [N II] profiles shown in Figure 5, taking into account that the measured FWHM of the line profile is due to the convolution of thermal, instrumental, turbulent, and expansion components. This can be approximated as:

$$\mathrm{FWHM}_{\mathrm{tot}}^2 = \mathrm{FWHM}_{\mathrm{th}}^2 + \mathrm{FWHM}_{\mathrm{ins}}^2 + \mathrm{FWHM}_{\mathrm{tur}}^2 + \mathrm{FWHM}_{\mathrm{exp}}^2 .$$

If we assume T_e of the order of 10,000 K, the resulting value for $\mathrm{FWHM}_{\mathrm{th}}$ is 5.7 km s^{-1} for [N II] and 21.2 km s^{-1} for Hα. The instrumental FWHM was 5.4 km s^{-1}. The measured FWHM was 0.55 Å for [N II] and 0.87 Å for Hα, thus, assuming that the turbulence component is negligible, $2 \times V_{\mathrm{exp}}[\mathrm{N\ II}] = 23.7$ km s^{-1} and $2 \times V_{\mathrm{exp}}(\mathrm{H}_\alpha) = 33.3$ km s^{-1}.

If we take a radius of 1.″5 for the bright inner nebular shell (from Bianchi et al. 1995 or Alves et al. 2000), corresponding to 0.075 or 0.09 pc at the distance of M15, $D = 10.3$ (Harris 1996) or 12.3 kpc (ABL00), respectively, and combine it with the expansion velocity from the [N II] nebular lines, we find

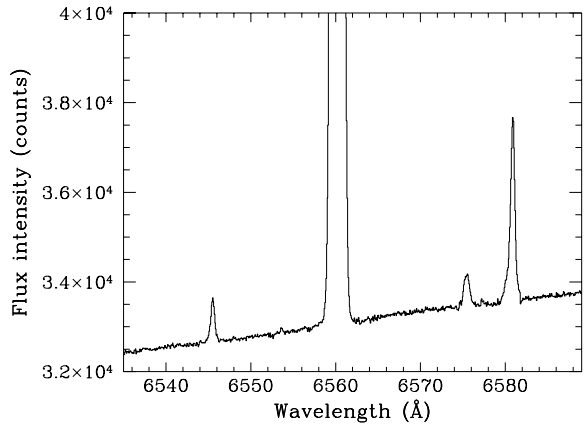

FIG. 5.—H_α and [N II] line profiles from the ground-based UES spectra.

an expansion age of 6000 (7100) yr. Using the expansion velocity from Hα, the age is lower: $\mathrm{Age}_{\mathrm{kinematic}}(\mathrm{H}\alpha) = 4270$ or 5070 yr, depending on the adopted distance. Figure 3 of ABL00 is color coded to show the emission of both Hα and [N II]. While most of the inner bipolar structure seems dominated by Hα emission, or by a combination of the three lines shown, [N II] is enhanced at the bright shock fronts at both ends of the elongated structure. Therefore, the lower [N II] velocity might reflect the fact that most of the emission comes from edge regions (where the projected expansion is lower), while the bulk of the Hα emission originates from more central areas (maximum projected velocity along the line of sight). Because our kinematic data do not have spatial resolution across the object, we cannot assess whether there is (acceleration or) deceleration within the shell.

We can expect the expansion to be slower in the beginning of the PN formation, when the fast stellar wind starts plowing into the slow thick wind from the AGB progenitor. This is also supported by observations, (see, e.g., Bianchi 1992), where measurements of the expansion of several PN show systematically higher velocities for larger objects. Therefore the kinematical age measured from the present expansion should be regarded as a lower limit to the life of the object in its current (post-AGB) stage.

5. DISCUSSION AND CONCLUSIONS

We performed an LTE spectral synthesis analysis of the UV spectrum of the central star of the PN K648 in the range 1200 Å $\leq \lambda \leq$ 3200 Å. We used $T_{\mathrm{eff}} = 37{,}000$ K and $\log g = 4.0$ taken from Heber et al. (1993). The models computed for these stellar parameters reproduce the stellar continuum very well over most of the observed range. A mismatch remains in the range of the G130L grating. Because the mismatch corresponds exactly to the spectral region covered by one grating (G130H), we cannot exclude reacquisition problems. From a model fit of the photospheric lines, we find an overabundance of helium (He/H = 0.6 by number) and of carbon (by a factor of 4 with respect to solar values), while silicon appears to be close to solar. There is also an indication of oxygen being significantly underabundant (1 dex or more) and Fe ≈ solar in the stellar photosphere.

Howard, Henry, & McCratney (1997; and previously Adams et al. 1984) measured abundances in the nebular gas of K648 and found oxygen and nitrogen underabundance with respect to solar, consistent with the photospheric abundances, but C and He abundances close to solar.

The ensemble of the results suggests (1) that the oxygen underabundance might reflect initial chemical composition (consistent with the very low metallicity of the M15 cluster) and (2) that processed material has not been mixed into the layers ejected to form the nebula.

The measured photospheric He and C overabundance, with O underabundance, suggests that the star experienced a third dredge-up event after the main nebular shell had been expelled (because C and He are not overabundant in the nebula).

The minimum core mass for the third dredge-up to occur is $M_{\mathrm{core}} \approx 0.54\ M_\odot$ for masses between 1.5–3 $M_\odot$ (Marigo, Girardi, & Bressan 1999a). Therefore, the fairly high mass (0.62 $M_\odot$) derived for the nucleus of K648 is consistent with the anomalous abundances in this scenario. The minimum *initial* masses for the third dredge-up to occur are between 1.1–1.5 $M_\odot$, decreasing with metallicity (Marigo et al. 1999a). Mazzitelli & D'Antona (1986) follow the entire evolution of a 3 $M_\odot$ star: at the end of the thick shell helium-burning phase a stratified composition of the core is obtained, where a carbon-rich mantel surrounds an oxygen-rich inner core. The boundary for the carbon-rich layer is 0.5 M_{core} (with overshooting) to 0.3 M_{core} (no overshooting), or ≈0.35–0.21 $M_\odot$. These authors also predict a final WD mass of ≈0.7 $M_\odot$. From recent model calculations and empirical calibrations of the initial-final mass relation (IFMR; Marigo 2001 and references therein), the inferred mass for the central star of K648 (0.62 $M_\odot$) implies a progenitor mass of $M_i \approx 2\ M_\odot$ if the metallicity were solar, but the value decreases to $M_i \approx 1.1$ for $Z = 0.004$ (P. Marigo 2001, private communication). Therefore, K648 must have evolved from a low-mass star. If we consider the main-sequence turn-off mass in M15 (0.8 $M_\odot$), even in the case of a binary coalesced at an early stage, the total mass of the parent star(s) should be lower than 1.6 $M_\odot$.

Further support for this evolutionary scenario comes from the measured stellar luminosity. The blackbody luminosity from our set of stellar parameters is $\log(L/L_\odot) = 3.45$.

This value is slightly lower than previous estimates: ABL00 estimated a luminosity $\log(L/L_\odot) = 3.78$, and Bianchi et al. (1995) derived $\log(L/L_\odot) = 3.67$. Our new value should be more precise because a synthetic spectrum was fitted to the UV observed spectrum, while previous estimates were based on spectrophotometry.

Post-AGB evolutionary tracks would predict a higher luminosity than we measure for the mass and temperature values derived in this paper (e.g., Vassiliadis & Wood 1994; Bloecker 1995), if it were a H-burning object. However, further He flashes in the post-AGB phase cause significant loops in the post-AGB evolutionary track on the Hertzsprung-Russell diagram (see, e.g., the evolution of a 0.6 $M_\odot$ object calculated by Schoenberner 1979). If a third dredge-up occurs, the mass-luminosity relation might also differ from what is usually assumed by post-AGB evolutionary models. Marigo et al. (1999b) show that the luminosity at quiescent phase (before the pulse) would be higher, but small-mass stars undergo a so-called "luminosity-dip" phase following the thermal pulse (TP), where the luminosity can drop by over a factor of 2 lower than the value given by the M_{core}-L relation.

In summary, the high core mass, the rather low luminosity, and the high He and C surface abundances seem to point toward a consistent evolutionary scenario for the object: a He-burning remnant that experienced a late thermal pulse and therefore a third dredge-up after expelling the nebular shell, with a low-mass progenitor. The mass of the remnant ($0.62\ M_{\odot}$) is high in comparison with average mass values of white dwarfs in globular clusters (see ABL00 and references therein), although we must recall that the uncertainties in this parameter are quite high. One possible explanation is that the object evolved from a former binary coalesced at an earlier stage. Also, it could be related to a lower mass-loss rate than usually assumed in the late-AGB evolutionary scenarios. Low mass loss would be expected given the low metallicity, at least in the post-AGB phase when the wind is driven by radiation pressure. The question remains whether the object has a binary origin. ABL00 did not detect photometric variability (from WFPC2 photometry) over timescales from 45 minutes to 7 days. The nondetection does not rule out the possibility of a binary (either seen pole-on or completely coalesced). We can conclude that comprehensive studies of this object have so far not provided any direct, decisive observational evidence for binarity or a merger, except for the bipolar morphology (Paper I), for which binarity is a most plausible but not unique explanation, and the fairly high mass of the remnant, although the probability of such origin is extremely high in the globular cluster environment.

The measured nebular expansion velocity, $V_{\rm exp}({\rm H}\alpha) = 16.7\ {\rm km\ s^{-1}}$, indicates a lifetime for the PN of ≥ 4270 yr. The post-AGB evolutionary models of Vassiliadis & Wood (1994) for He-burning stars indicate a timescale of about 2000 yr, for an $M = 0.6\ M_{\odot}$ remnant at the $T_{\rm eff}$ of the K648 central star, for $Z = 0.016$, and slightly lower at lower metallicity.

The measured lifetime is then about a factor of 2 longer than evolutionary model predictions. The discrepancy is reminiscent of the "lazy evolution" often invoked to explain properties of stars in globular clusters. However, a small uncertainty in the mass reflects a large change in the evolutionary timescale, so a factor of 2 cannot be claimed to be significant. Buell et al. (1997) performed calculations for two evolutionary scenarios that could possibly reproduce the object of this study. In the first one (prompt scenario) the planetary nebula is ejected after a helium shell flash; in the second case (delayed scenario) a third dredge-up occurs before the envelope is ejected. Both models predict a carbon-rich star during a stage that lasts only a few hundred years, because of subsequent mass loss after the dredge-up. However, in both models the predicted luminosity is much higher than the value estimated in this paper (and in previous works), and the mass of the remnant significantly lower; therefore a direct comparison with the predicted timescales is not possible.

From the C IV line profile we derived a wind terminal velocity of $V_{\infty} = 1600 \pm 150$ km s^{-1} and $\dot{M} \times Q_i$ (C IV) $= 3.2 \pm 1.1\ 10^{-11}\ M_{\odot}\ {\rm yr^{-1}}$. From the stellar parameters derived in previous sections, we derive an escape velocity (corrected for radiation pressure) of $V_{\rm esc} = 425$ km s^{-1}. The ratio V_{∞} to $V_{\rm esc}$ is then ≈ 3.8, larger than the radiation pressure wind theory prediction (≈ 3.1) for high-luminosity stars, but close to typical ratios for central stars of planetary nebulae (Heap 1982; Pauldrach et al. 1988).

Far-UV data are planned for the current cycle with the *FUSE* satellite to directly measure the wind ionization structure. An independent NLTE analysis of new optical data and of the existing *HST* data is also planned (Rauch et al. 2001; see also Rauch, Bianchi, & Heber 2000).

We are very grateful to Paola Marigo for extremely useful discussions about the evolutionary aspects. Support for this work was provided by NASA through grant number NRA 99-01 LTSA-029 (L. B.) and grant PB 97-1435-C02-01 from the Dirección General de Enseñanza Superior. The authors are grateful for the allocation of service time at the WHT for this snapshot proposal.

REFERENCES

Alves, D. R., Bond, H., & Livio, M. 2000, AJ, 120, 2044 (ABL00)
Adams, S., Seaton, M. J., Howarth, I. D., Auriere, M., & Walsh, J. R. 1984, MNRAS, 207, 471
Aurière, M., Adams, S., & Seaton, M. J. 1983, MNRAS, 205, 571
Aurière, M., & Cordoni, J.-P. 1981, A&AS, 46, 347
Behr, B. B., Cohen, J. G., & McCarthy, J. K. 2000, ApJ, 531, L37
Bianchi, L. 1992, A&A, 260, 314
Bianchi, L., et al. 2000, ApJ, 538, L57
Bianchi, L., Ford, H., Bohlin, R., Paresce, F., & de Marchi, G. 1995, A&A, 301, 537 (Paper I)
Bloecker, T. 1995, A&A, 299, 755
Bohlin, R. C. 1996, AJ, 111, 1743
Bohlin, R. C., Lindler, D. J., & Keyes, C. D. 1995, Cycle 4 Photometric Calibration of the FOS (Instrum. Sci. Rep. CAL/FOS-144) (Baltimore: STScI)
Buell, J. F., Henry, R. B. C., Baron, E., & Kwitter, K. B. 1997, ApJ, 483, 837
Gillett, F. C., et al. 1989, ApJ, 338, 862
Groenewegen, M., & Lamers, H. J. G. L. M. 1989, A&AS, 79, 359 (GL89)
Groenewegen, M., Lamers, H. J. G. L. M., & Paudrach, A. W. A. 1989, A&A, 221, 78
Harris, W. E. 1996, AJ, 112, 1487
Hawley, S. & Miller, J. 1978, IAU Symp. 76, Planetary Nebulae, ed. Y. Terzian (Dordrecht: Reidel), 245
Heap, S. R. 1982, in IAU Symp. 99, Wolf-Rayet Stars: Observations, Physics, Evolution, ed. C. H. de Loore & A. J. Willis (Dordrecht: Reidel), 423
Heber, U., Dreizler, S., & Werner, K. 1993, Acta Astron., 43, 337
Howard, J. W., Henry, R. B. C., & McCratney, S. 1997, MNRAS, 284, 465
Jacoby, G. H., et al. 1997, AJ, 114, 2611
Joy, A. H. 1949, ApJ, 110, 105
Lamers, H. J. G. L. M., Cerruti-Sola, M., & Perinotto, M. 1987, ApJ, 314, 726
Kingsburgh, R. L., & Barlow, M. J. 1992, MNRAS, 257, 317
Kudritzki, R.-P., Pauldrach, A. W. A., Puls, J., & Abbott, D. C. 1989, A&A, 219, 205
Kurucz, R. L. 1993, in IAU Coll. 138, Peculiar versus Normal Phenomena in A-Type and Related Stars, ed. M. M. Dworetsky, F. Castelli, & R. Faraggiana (ASP Conf. Ser. 44) (San Francisco: ASP), 87
Kurucz R. L. & Avrett E. H. 1981, SAO Special Rep., 391
Marigo, P. 2001, A&A, 370, 194
Marigo, P., Girardi, L., & Bressan, A. 1999a, A&A, 344, 123
Marigo, P., Girardi, L., Weiss, A., & Groenewegen, M. A. T. 1999b, A&A, 351, 161
Mazzitelli, I., & D'Antona, F. 1986, ApJ, 308, 706
Pauldrach, A., Puls, J., Kudritzki, R.-P., Mendez, R., & Heap, S. R. 1988, A&A, 207, 123
Peimbert, M. 1973, Mem. Soc. R. Sci. Liège, 5, 307
Peña, M., Torres-Peimbert, S., & Ruiz, M. T. 1992, A&A, 265, 757
Rauch, T., Bianchi, L., & Heber, U. 2000, Astron. Ges. Abstr. Ser., 17, 5
Rauch, T., Heber, U., & Werner, K. 2001, in preparation
Schneider, S., Terzian, Y., Purgathofer, A., & Perinotto, M. 1983, ApJS, 52, 399
Schoenberner, D. 1979, A&A, 79, 108
Torres-Peimbert, S., & Peimbert, M. 1979, Rev. Mexicana Astron. Astrofis., 4, 341
Vassiliadis, E., & Wood, P. R. 1994, ApJS, 92, 125
Webbink, R. H. 1985, in IAU Symp. 113, Dynamics of Star Cluster, ed. J. Goodman & P. Hut (Dordrecht: Reidel), 541